JACS
JOURNAL OF THE AMERICAN CHEMICAL SOCIETY

ARTICLE

pubs.acs.org/JACS

Stochastic Amperometric Fluctuations as a Probe for Dynamic Adsorption in Nanofluidic Electrochemical Systems

Pradyumna S. Singh,[†,‡] Hui-Shan M. Chan,[†] Shuo Kang,[‡] and Serge G. Lemay[*,‡]

[†]Kavli Institute of Nanoscience, Delft University of Technology, Lorentzweg 1, 2628 CJ Delft, The Netherlands

[‡]MESA+ Institute for Nanotechnology, University of Twente, 7500 AE Enschede, The Netherlands

Supporting Information

ABSTRACT: Adsorption of analyte molecules is ubiquitous in nanofluidic channels due to their large surface-to-volume ratios. It is also difficult to quantify due to the nanometric scale of these channels. We propose a simple method to probe dynamic adsorption at electrodes that are embedded in nanofluidic channels or which enclose nanoscopic volumes. The amperometric method relies on measuring the amplitude of the fluctuations of the redox cycling current that arise when the channel is diffusively coupled to a bulk reservoir. We demonstrate the versatility of this new method by quantifying adsorption for several redox couples, investigating the dependence of adsorption on the electrode potential and studying the effect of functionalizing the electrodes with self-assembled monolayers of organothiol molecules bearing polar end groups. These self-assembled monolayer coatings are shown to significantly reduce the adsorption of the molecules on to the electrodes. The detection method is not limited to electrodes in nanochannels and can be easily extended to redox cycling systems that enclose very small volumes, in particular scanning electrochemical microscopy with nanoelectrodes. It thus opens the way for imaging spatial heterogeneity with respect to adsorption, as well as rational design of interfaces for redox cycling based sensors.

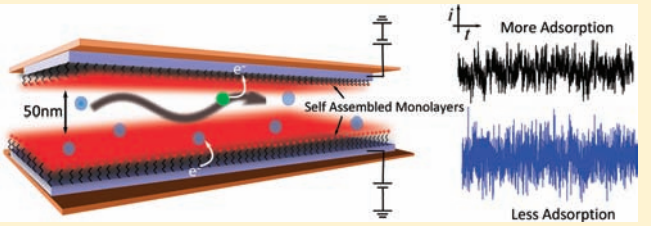

INTRODUCTION

There is at present considerable interest in the use of nanochannels and nanofluidic devices as selective and sensitive detection tools for analytical and bioanalytical applications.[1,2] However, as detection volumes shrink further into the nanoscale regime, the increasing surface-to-volume ratio means that molecules being transported through these channels have a greater interaction with the channel surface.[3] Consequently, molecules tend to adsorb nonspecifically to the channel walls or to the sensor elements embedded within these channels (e.g., electrodes). This can have severe consequences on the sensor response, especially in cases where this response is limited by mass transport of the molecules to the sensing element. For example, in recent experiments involving single-molecule electrochemical detection, it was found that the signal was significantly attenuated on account of reversible adsorption of analyte redox molecules.[4] It is thus desirable to develop new protocols to minimize adsorption and, correspondingly, to develop new techniques to quantify it.

To date, the most common approach for measuring adsorption in nanochannels has been through the use of optical techniques, most notably fluorescence correlation spectroscopy (FCS). FCS reveals adsorption to channel walls by measuring the decrease in the effective diffusion constant, D_{eff}, of molecules in channels.[5−7] In many instances, however, optical methods can prove too cumbersome or even impossible to implement, such as for the case of opaque nanostructures. This is also true of techniques such as ellipsometry and surface plasmon resonance (SPR), which, while widely applied to the characterization of thin films on metal substrates, are difficult to exploit for the study of dynamic adsorption in nanochannels with sub-monolayer coverage. Similarly, while a variety of electrochemical methods can be employed to probe adsorption at electrodes, they are difficult to implement within nanochannels.[8−11] Our group recently introduced an electrochemical analogue of FCS, electrochemical correlation spectroscopy (ECS), which can be used to determine D_{eff} through amperometric measurements of the redox cycling current instead of a fluorescent signal.[12] ECS is in principle well-suited for quantifying the adsorption of reversible or quasi-reversible redox species at electrodes and can be applied to all redox cycling systems that enclose a small fluidic volume including thin-layer cells (TLCs), interdigitated electrodes (IDEs), and scanning electrochemical microscopy (SECM) systems. In practice, however, the routine measurement of D_{eff} as a characterization tool is limited by the high quality and long duration of the amperometric measurements that are needed to extract accurate values. Furthermore, a proper assessment of the spectra requires precise knowledge of the geometry of the dual electrodes and considerable amounts of nontrivial mathematics. This is particularly limiting in the SECM case, where spatial mapping of heterogeneities in the adsorption properties of surfaces would become possible were a more rapid and robust measurement method available.

Received: July 20, 2011
Published: September 29, 2011

dx.doi.org/10.1021/ja2067669 | J. Am. Chem. Soc. 2011, 133, 18289–18295

Herein, we introduce theoretically and experimentally a simpler, more generally applicable and, consequently, more powerful formulation of ECS that permits rapid quantification of reversible adsorption and that can be implemented straightforwardly in any redox cycling geometry. Like frequency-based ECS, the method relies on measuring the *fluctuations* in the faradaic current. Instead of a full spectral analysis, however, the degree of adsorption is extracted directly from the amplitude and/or a cross-correlation analysis of the fluctuations. A key advantage of the method is that, using only steady-state measurements, the absolute number of adsorbed molecules can be directly determined. We first demonstrate that the amplitude- and frequency-based approaches yield consistent results. We then apply the new approach to characterize adsorption for several adsorbates under a range of experimental conditions. In particular, we explore the use of thiolate self-assembled monolayers (SAMs) to functionalize Pt electrodes in order to minimize adsorption of electroactive molecules from aqueous solutions. The self-assembly of monolayers of organothiol molecules on noble or coinage metal electrodes is among the most powerful and versatile ways of modifying electrode surfaces; this is because SAMs on metal surfaces are easy to prepare and organize into (semi)crystalline structures spontaneously and they can be easily used to tune interfacial properties by choice of suitable terminal end group. While many investigations have dealt with the effects of SAMs on heterogeneous electron-transfer kinetics, much less is known about their properties with respect to dynamic adsorption of molecules at SAM-functionalized interfaces. Most studies on adsorption at SAM-modified interfaces have dealt with large macromolecular species such as proteins,[13,14] nanoparticles,[15−17] and surfactants.[18] To our knowledge, this is the first study to explore the adsorption of small redox active molecules at SAM interfaces.

THEORY

We introduce here the theoretical basis of the new method, the particular conditions under which it is applicable and its limitations. The specific geometry used in the present study consists of two closely spaced plane-parallel Pt electrodes embedded in a nanofluidic channel, as sketched in Figure 1a. The electrodes are biased in such a way that a diffusing electroactive molecule can be reduced at one electrode and oxidized at the other, thus resulting in an amplification of the electrochemical current. This is equivalent to the positive-feedback mode in SECM. The currents through the oxidizing electrode and the reducing electrode are independently measured, as seen in Figure 1b. The average redox cycling faradaic current so generated is given by $\langle I_F \rangle = i_p \langle N \rangle$, where i_p is the current per molecule and $\langle N \rangle$ is the average number of molecules in the active region of the device (defined as the volume bounded by the region of overlap between the two electrodes). The brackets denote time averaging. For purely diffusive transport, $i_p = neD/z^2$ where n is the number of electrons transferred per molecule, $-e$ is the charge on an electron, D is the diffusion constant of the redox species, and z is the spacing between the two electrodes. However, i_p can be lowered below this maximum value due to electron-transfer kinetics limitation, intermittent adsorption, and so on.

Randomly diffusing molecules that contribute to the electrochemical current are capable of entering and exiting the detection volume. The exact number of molecules in the detection volume at any given instant, $N(t)$, therefore fluctuates in time around its mean value, $\langle N \rangle$. Since the measured electrochemical current is simply the sum of the individual currents contributed by each molecule, the current also fluctuates in time according to $I_F(t) = i_p N(t)$.

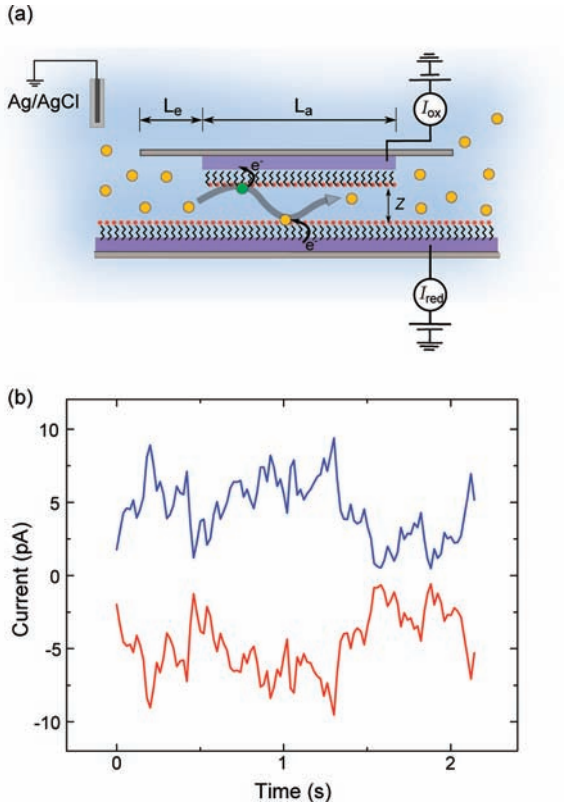

Figure 1. (a) Schematic of a nanofluidic thin-layer cell with two independently addressable electrodes functionalized with SAMs and separated by a nanometer scale distance, z. L_e is the length of the access nanochannel leading to the active region while the active region has a length L_a. (b) Fluctuations in the amperometric traces obtained for 100 μM $Fc(MeOH)_2$. The DC component has been offset to focus on the fluctuations. The amplitudes of the traces for the oxidizing (blue) and reducing (red) electrodes are directly correlated, but the currents are opposite in sign as expected for redox cycling.

What is the magnitude of these fluctuations? Elementary statistics tells us that the probability P_N of finding exactly N molecules in a small volume in equilibrium with a large reservoir is given by the Poisson distribution, $P_N = \langle N \rangle^N \exp(-\langle N \rangle)/N!$. The variance of this distribution, $\langle (N(t) - \langle N \rangle)^2 \rangle$, is equal to $\langle N \rangle$. The corresponding rms noise amplitude for the faradaic current is thus $I_{F,rms} = i_p [\langle (N(t) - \langle N \rangle)^2 \rangle]^{1/2} = i_p \langle N \rangle^{1/2}$. Taking the ratio of $\langle I_F \rangle$ and $I_{F,rms}$ and rearranging yields, the simple result for the number of molecules

$$\langle N \rangle^{amp} = \langle N_{ads} \rangle + \langle N_{sol} \rangle = \frac{\langle I_F \rangle^2}{I_{F,rms}{}^2} \quad (1)$$

Here the superscript "amp" indicates that this is the value of $\langle N \rangle$ determined from the *amplitude* of the fluctuations, as opposed to the alternative frequency-based method described further below. Equation 1 shows that $\langle N \rangle$ can be determined directly from two experimentally measurable quantities, $\langle I_F \rangle$ and $I_{F,rms}$. Here we have also explicitly highlighted the fact that the total number of molecules in the channel, $\langle N \rangle$, includes both the molecules

adsorbed on the electrodes, $\langle N_{ads}\rangle$, as well as molecules freely diffusing in solution, $\langle N_{sol}\rangle$. If no adsorption takes place on the electrodes ($\langle N_{ads}\rangle = 0$), then the number of molecules determined from the above ratio of $\langle I_F\rangle$ and $I_{F,rms}$ should be equal to the number expected from the bulk concentration; i.e., $\langle N\rangle = \langle N_{sol}\rangle = CVN_A$, where C is the bulk concentration of the analyte, V is the volume of the active region of the device, and N_A is Avogadro's constant. If there is adsorption, however, then $\langle N\rangle$ will be higher than expected from the bulk concentration, and this can be detected as decreased noise amplitude through eq 1. This is the essence of the new approach we propose. Note that $\langle N_{ads}\rangle$ has contributions from molecules adsorbed at both electrodes. It can be expressed in terms of the surface concentration of molecules on the electrodes, $\langle N_{ads}\rangle = N_A A(\Gamma_{ox} + \Gamma_{red})$, where A is the area of overlap between the top and bottom electrodes and Γ_{ox} and Γ_{red} are the surface concentrations of the oxidized and reduced forms, respectively.

In practice, the measured fluctuations include a redox cycling component, as per eq 1, as well as unwanted instrumental noise. Any such excess noise increases the apparent value of $I_{F,rms}$ and leads to an underestimation of the amount of adsorbed molecules. This potential source of systematic error can however be eliminated by taking advantage of the redox cycling configuration, in which symmetric reduction and oxidation processes take place at the two working electrodes. $I_{ox}(t) = u_{ox}(t) + I_F(t)$ and $I_{red}(t) = u_{red}(t) - I_F(t)$ represent the current at the oxidizing and reducing electrodes, respectively. Here $u_{ox}(t)$ and $u_{red}(t)$ are the random instrumental noise at the two channels; the faradaic fluctuations, $I_F(t)$, are anticorrelated between the two electrodes while $u_{ox}(t)$ and $u_{red}(t)$ are uncorrelated with each other as well as with $I_F(t)$. It directly follows (see Supporting Information for details) that $\langle I_{ox}I_{red}\rangle = -\langle I_F\rangle^2 - I_{F,rms}^2$, independently of the amplitudes of the instrumental noise, $u_{red}(t)$ and $u_{ox}(t)$. Combining this result with eq 1 yields a robust expression in the presence of excess noise,

$$\langle N\rangle^{amp} = \langle N_{ads}\rangle + \langle N_{sol}\rangle = -\left(1 - \frac{\langle I_{ox}I_{red}\rangle}{\langle I_{ox}\rangle\langle I_{red}\rangle}\right)^{-1} \quad (2)$$

Equation 2 is the preferred method of evaluating $\langle N\rangle$. Alternately, in experimental situations where I_{ox} and I_{red} cannot be measured simultaneously, eq 1 can instead be employed with either I_{ox} or I_{red} taking the place of I_F. This is valid so long as fluctuations in $N(t)$ are the dominant source of noise and that other contributions to the noise are relatively insignificant. To see how this condition can be satisfied, note that eq 1 can be rearranged to yield $I_{F,rms}/\langle I_F\rangle = 1/\langle N\rangle^{1/2}$. That is, the relative size of the fluctuations becomes increasingly important as the average number of molecules in the system decreases. For sufficiently low detection volumes and/or concentrations, diffusion noise dominates over noise from extraneous sources such as the measurement instrumentation. Because the active volume of the nanofluidic devices employed here is only ca. 1 fL (10^{-15} L), this condition is easily satisfied even at high (~1 mM) concentrations using conventional potentiostats, and eq 1 and eq 2 yield identical results in practice in our case.

The derivation leading to eq 2 is general in that it is independent of kinetic limitations due to electron transfer, adsorption, and so forth. Several criteria however have to be fulfilled in order for the above argument to be valid. First, this method is only valid for redox couples that can redox cycle, i.e., redox couples whose oxidized and reduced forms are stable on a time scale longer than the residence time of molecules inside the active volume of the device. Second, the geometry of the system should be such that the residence time in the active region is significantly longer than the shuttling time between the two electrodes. This ensures that additional noise due to the randomness of the shuttling process itself is negligible.[19,20] Third, the current must be measured sufficiently fast that the full spectrum of the diffusive fluctuations is captured. Measurements that average part of the diffusive fluctuations will lead to an overestimate of $\langle N\rangle$. This criterion is easily met in practice because the power density falls off rapidly as $f^{-3/2}$ at high frequencies, leading to negligible error as long as the measurement system has a bandwidth significantly greater than the characteristic frequency f_0 (defined as follows). Lastly, the adsorption must be reversible with kinetics sufficiently fast that they are averaged over during the amperometric measurement (a combination which we refer to as dynamic adsorption). As a result, the effect of adsorption is to increase $\langle N\rangle$ and decrease i_p, as per the derivation above.

While Poisson statistics describe the magnitude of the fluctuations, they do not reveal their time evolution. Similar information about adsorption can however be obtained by analyzing the *time scale* of the fluctuations. This alternative method was described in detail in an earlier study.[12] In brief, the spectrum of the fluctuations contains detailed information about the dynamics of redox molecules as they diffuse in and out of the active region of the device. For a detection volume in the shape of a long channel, it was shown theoretically and experimentally that the power spectral density, $S(f)$, is, to a good approximation, of the form

$$S(f) = \frac{S_0}{1 + \left(f/f_0\right)^{3/2}} \quad (3)$$

where S_0 and f_0 are constants. That is, the noise power exhibits a plateau at low frequencies and declines as $f^{-3/2}$ at high frequencies. The crossover frequency, f_0, is a measure for how fast the current fluctuates and is given by[12] $f_0 = (D_{eff}/\pi)\ (3/L_a{}^2(L_a + 6L_e))^{2/3}$. Here L_a and L_e are geometry-specific parameters, as illustrated in Figure 1a, while D_{eff} is the effective diffusion constant. The value of D_{eff} decreases with increasing adsorption, since diffusion is momentarily suspended each time a molecule is adsorbed. D_{eff} is in fact directly related to the number of molecules in the active volume via $D_{eff}/D = \langle N_{sol}\rangle/\langle N\rangle$, where D is the true diffusion constant of the redox species. It follows that the occurrence of adsorption can be detected by an examination of D_{eff}. Combining these results yields a simple expression for the total number of molecules present in the channel as determined from analysis in the frequency domain,

$$\langle N\rangle^{freq} = \langle N_{ads}\rangle + \langle N_{sol}\rangle = CVN_A \frac{f_0^{ideal}}{f_0^{meas}} \quad (4)$$

where $f_0{}^{meas}$ is the measured crossover frequency and $f_0{}^{ideal}$ is the calculated value assuming no adsorption ($D_{eff} = D$). In what follows, we demonstrate experimentally that eq 2 and eq 4, which quantify adsorption based on an analysis of the amplitude and the frequency dependence of the fluctuations, respectively, yield consistent results, $\langle N\rangle^{freq} = \langle N\rangle^{amp}$.

EXPERIMENTAL SECTION

Materials and Reagents. The organothiol molecules used for electrode modification were 3-mercaptopropionic acid (3-MPA, ≥99%, Aldrich), 6-mercaptohexanol (MHX, 99%, Aldrich), 4-mercaptobenzoic

acid (MBA, 99%, Aldrich), and 1-propanethiol (1-PT, 99%, Aldrich). All of the thiols were used as received. Ferrocene (Fc, ≥ 98%), ferrocenemethanol (FcMeOH, 97%), ferrocenedimethanol ($Fc(MeOH)_2$, 98%), and hexammineruthenium(III) chloride ($Ru(NH_3)_6Cl_3$, 98%) were purchased from Sigma-Aldrich and used as received. Potassium chloride (KCl), tetrabutylammonium hexafluorophosphate (Bu_4NPF_6, electrochemical grade), and sulfuric acid (H_2SO_4, 99.999%) were purchased from Sigma-Aldrich. Acetonitrile (ACN) solutions were prepared using HPLC grade solvent (≥99.9%). All aqueous solutions were prepared using 18.2 MΩ·cm Milli-Q water. Absolute analytical grade ethanol was used to prepare the thiol solutions.

SAM Functionalization. Thiolate SAMs on electrochemical interfaces have been intensively investigated and reviewed over the past 2 decades,[21] and, while most attention has been paid to the formation of SAMs on Au electrodes, several studies have shown the feasibility of the formation of stable, dense, and highly ordered SAMs on single-crystal[22−24] and polycrystalline thin-film Pt electrodes.[25−27] The thiol functionalization was achieved by first cleaning the electrodes with 0.5 M H_2SO_4 (see the Supporting Information). After this, 1−10 mM ethanol solutions of thiols were flowed into the device. Once the device was filled with the thiol solution, the device together with the PDMS reservoir were sealed in parafilm and left overnight. Before use, the devices were flushed with ethanol to remove any extra unadsorbed SAM molecules. The formation of thiol monolayers was evidenced and characterized by the decrease in the double-layer capacitance and the diffusion-limited redox cycling current, i_{lim}, for the SAM-coated electrodes compared to the bare electrodes (see the Supporting Information).

Nanofluidic Devices. The fabrication of the nanofluidic devices employed herein has been described elsewhere.[28] In brief, a three layer sandwich structure consisting of Pt−Cr−Pt was fabricated using evaporation and lithographic patterning. The devices were encased in sputtered SiO_2 (550 nm thick) or Si_3N_4 using PECVD. The geometry of the devices is illustrated in Figure 1a. The thickness of the Cr layer determines the electrode spacing, z. The active region of the device is defined as the volume enveloped by the two overlapping top and bottom electrodes. Two sets of devices were used for experiments described herein. The first type, hereon referred to as Type 1, had an active region of dimensions 10 μm × 1.5 μm × 50 nm. In these devices, two 1 × 1 μm^2 access holes were patterned at a distance of 8 μm on either side of the top electrode for coupling with the bulk reservoir. L_e = 8 μm and L_a = 10 μm in terms of the geometry parameters of Figure 1a. For this geometry, a concentration of 100 μM corresponds to 4.5 × 10^4 molecules in the active region. In the second type, hereon referred to as Type 2, the active region had dimensions 10 μm × 3 μm × 70 nm. In this set of devices, L_e = 2 μm and L_a = 10 μm with the access holes being 4 × 4 μm^2. For this geometry, 100 μM corresponds to 1.3 × 10^5 molecules in the active region.

Electrochemical Measurements. The electrochemical measurements were performed using a CHI832B bipotentiostat (CH Instruments). The two working electrode terminals were connected to the top and bottom electrodes. For experiments in aqueous media, a standard Ag/AgCl electrode (3 M NaCl, BASi) served both as reference and counter electrode. This configuration is appropriate since the current flowing through the reference electrode is ≤120 pA, much smaller than the redox cycling current.[28] The reference electrode was immersed in a PDMS reservoir that contacted the device. For experiments in acetonitrile, the reference electrode was a silver wire in contact with a solution of 0.10 M Bu_4NPF_6 and 0.010 M $AgNO_3$, in ACN. In aqueous studies 1 M KCl was the supporting electrolyte, while 0.10 M Bu_4NPF_6 was used in acetonitrile.

Amperometric traces were acquired by having one electrode poised at an oxidizing potential and the other at a reducing potential. Unless otherwise stated, the oxidizing potential was +0.5 V and the reducing potential was 0 V, in aqueous solutions. In nonaqueous media, the oxidizing and reducing potentials were +0.4 and −0.05 V, respectively. Typically 900 s of a trace were acquired at 50 Hz sampling rate (with 150 Hz low-pass filters). After detrending, the first 100 s of data was ignored (to account for various transients due to electronic setups) and the remaining data were divided into segments of 100 s for each of which the ratio of $\langle I_{ox} \rangle$ to $I_{F,rms}$ was computed and finally averaged. A cross-correlation analysis was also performed for each data set using eq 2. There was negligible difference (<1%) between values of $I_{F,rms}$ obtained directly and via cross-correlation analysis. For each 100 s trace the power spectral density (PSD) was also computed and finally the PSDs were averaged. To determine the effects of various SAMs, each of the aforementioned measurements were performed on the bare as well as SAM-functionalized electrodes. After performing experiments on the bare electrodes, the cleaning procedure with H_2SO_4 was undertaken following which the device was functionalized with the requisite SAMs and the experiments repeated.

RESULTS AND DISCUSSIONS

Figure 2a shows the raw redox cycling amperometric traces obtained in a Type 1 device for 50 μM $Fc(MeOH)_2$ in 1 M KCl on bare Pt electrodes and on electrodes functionalized with 3-mercaptopropionic acid (3-MPA). A comparison of the traces reveals two key features: first, it is apparent that the noise amplitude is higher for the traces obtained at functionalized electrodes compared to the traces at bare electrodes. Second, the time scale of the fluctuations is more rapid for the functionalized electrodes.

Using the geometry parameters of the active region of the Type 1 devices, a concentration of 50 μM $Fc(MeOH)_2$ corresponds to $\langle N_{sol} \rangle$ = 2.3 × 10^4 molecules in the active region of the device. From eq 2, we calculate $\langle N \rangle^{amp}$ = 1.5 × 10^5 molecules for bare Pt electrodes: a nearly 7-fold increase compared to the expected value that can be attributed to adsorption of the molecules on the electrodes. Using the same analysis for the 3-MPA functionalized electrodes, we calculate $\langle N \rangle^{amp}$ = 5.0 × 10^4 molecules, only twice the theoretically expected value in the absence of adsorption and three times less than the bare electrodes. Such an increase in the noise amplitude is consistent with a reduced number of molecules in the channel due to lessened adsorption.

To reconcile the second observation regarding the time scale of the fluctuations, we compare the above results with power spectral analysis of the same data. Figure 2b shows power spectral densities computed from the amperometric traces. As expected, the PSDs show a flat plateau at low frequencies and $f^{-3/2}$ decay at higher frequencies. Importantly, the corner frequency, f_0^{meas}, increases after SAM functionalization, consistent with the more rapid fluctuations visible in Figure 2a. Fits of the data to eq 3 yield f_0^{meas} = 0.21 and 0.68 Hz for the bare and 3-MPA functionalized electrodes, respectively. For comparison, the geometry parameters for Type 1 devices yield f_0^{ideal} = 1.37 Hz. As discussed above, the lower values of f_0^{meas} can be attributed to the adsorption of $Fc(MeOH)_2$ onto the electrodes.[12] The increased crossover frequency for the SAM-functionalized electrodes implies faster diffusion and, correspondingly, reduced adsorption. The ideally expected value of the crossover frequencies is also nearly 7× higher than that observed at bare electrodes and 2× higher than that at SAM-functionalized electrodes, consistent with the numbers obtained from the analysis of the fluctuation amplitudes.

To further compare the amplitude- and frequency-based methods, we compare the number of molecules obtained from eq 2 and eq 4 for a variety of situations. Figure 3 shows a plot

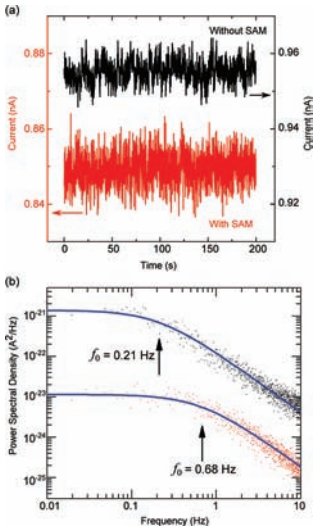

Figure 2. (a) Amperometric traces obtained with 50 μM $Fc(MeOH)_2$ under redox cycling conditions at bare Pt electrodes (black trace) and at 3-MPA-functionalized electrodes (red trace) in Type 1 devices. (b) Power spectral densities for the corresponding traces in a. The spectrum for the bare electrode (black) has been offset by a factor of 10^2 for clarity. The blue lines are fit to eq 3, which yields f_0^{bare} = 0.21 Hz and f_0^{SAM} = 0.68 Hz.

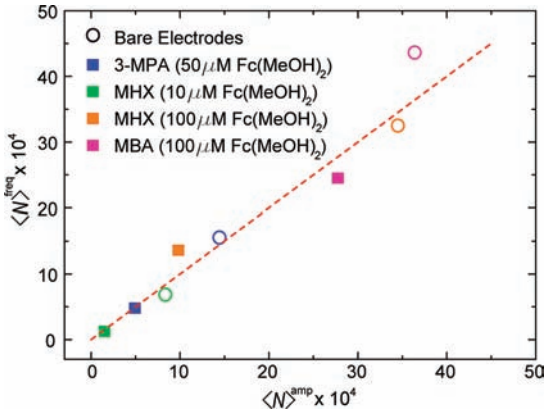

Figure 3. Comparison of $\langle N\rangle^{freq}$ obtained from eq 4 and $\langle N\rangle^{amp}$ calculated from eq 2. The circles are data obtained at bare Pt electrodes, and the solid squares are the corresponding data obtained at SAM-functionalized electrodes. All data were obtained on separate devices of Type 1.

comparing $\langle N\rangle^{freq}$ and $\langle N\rangle^{amp}$ for various concentrations of $Fc(MeOH)_2$ at bare Pt electrodes and electrodes functionalized with various SAMs. f_0^{meas} was extracted from fit to the power spectra as shown in Figure 2, while $\langle N\rangle^{amp}$ was extracted from the same time traces using eq 2. The data are clustered around the dashed line (slope = 1) representing good agreement between these two different methods. Thus, this analysis independently validates the equivalence of spectral analysis with the simpler and more general approach proposed here. The new method therefore provides a convenient means of overcoming limitations of frequency-based ECS as described in the Introduction.

While there is some scatter in the amount of adsorption seen on bare electrodes, indicating that adsorption is sensitive to sample history, all the SAMs with polar end groups result in lowering the adsorption of $Fc(MeOH)_2$ compared to the bare electrodes. Table 1 shows a comparison of the calculated $\langle N\rangle$ for devices with bare Pt electrodes and with several different SAM functionalizations. It is apparent that MHX and 3-MPA are most effective in preventing the adsorption of $Fc(MeOH)_2$ onto Pt electrodes. The use of 3-MPA has been previously investigated with a view to enhance the electrochemical detection of dopamine in both fundamental and sensor-based experiments.[29−31] It has been suggested that adsorption onto metal electrodes is governed by hydrophobic interactions between the redox moiety and the electrode. While the molecular mechanism of adsorption remains unknown, we can speculate that polar hydrophilic end-groups such as in the SAMs tried here disrupt the hydrophobic interactions between $Fc(MeOH)_2$ and the electrode surface, thereby preventing adsorption. This view is supported by results obtained on electrodes functionalized with 1-PT. Although 1-PT has the same length of the alkane backbone as 3-MPA, it does not have a polar terminal group like −COOH. As can be seen in Table 1, 1-PT has the opposite effect of enhancing adsorption. Unlike their behavior in aqueous solution, 3-MPA and MHX do not mitigate adsorption from acetonitrile solutions. This is not surprising since it has been known that superior solvation of the SAMs by acetonitrile renders the SAMs permeable to both ferrocene and ferricenium ions.[32] This is also evidenced by the negligible change in the diffusion-limited current and double-layer capacitances in acetonitrile for the SAM-functionalized electrodes compared to the bare electrodes (see the Supporting Information). While this further supports an important role for hydrophobic interactions, such an interpretation can only be considered tentative, since it is well-known that smaller SAMs such as 3-MPA or 1-PT tend to form highly disordered SAMs in water.[33] This disorder might expose the hydrophobic backbone of the SAMs in equal measure for the two cases.

A key advantage of the present method over the frequency-based approach is that one does not need to know the diffusion constant of the redox species in order to determine whether or not adsorption is taking place. To test this, we compared the adsorption properties of $Fc(MeOH)_2$ with ferrocene (Fc) and ferrocene methanol Fc(MeOH). Due to the low solubility of Fc in water, we performed these experiments in ACN. The results are summarized in Table 2. The crossover frequencies show a pronounced trend with the number of MeOH groups. Without the knowledge of their respective diffusion constants, this might suggest that the unsubstituted Fc tends to adsorb less (due to higher f_0^{meas}). However, f_0 also scales with the bare diffusion coefficient as D^{-1}, and this fully accounts for the observed shift in f_0, as seen from the values of $\langle N\rangle^{amp}$ and $\langle N\rangle^{freq}$ in Table 2. Besides lending additional support to the equivalence between ECS and the present analysis, this shows that one need not have prior knowledge of the diffusion constants to assess adsorption using the amplitude-based technique. Interestingly, the data further suggest that hydrophilic substituents on the cyclopentadienyl ring do not affect the adsorption behavior of Fc molecules from aprotic solvents.

Because the present method is general and valid for all magnitudes of i_p, it is also well-suited to studying the potential dependence of adsorption properties. Figure 4 shows data for $\langle N\rangle^{amp}$ obtained as a function of electrode potential for $Fc(MeOH)_2$ and $Ru(NH_3)_6^{3+}$. Due to variability from device to device, only one experiment is shown here. However, other experiments show the same trends. For both molecules it is apparent that the amount of

Table 1. $\langle N \rangle^{amp}$ from Equation 2 in Devices with Bare and SAM-Functionalized Electrodes

SAM	concn $Fc(MeOH)_2$ (μM)	$\langle N \rangle^{amp}$ (on bare Pt)	$\langle N_{ads} \rangle / \langle N_{sol} \rangle$	$\langle N \rangle^{amp}$ (with SAM)	$\langle N_{ads} \rangle / \langle N_{sol} \rangle$
3-MPA	50	1.5×10^5	5.3	5.0×10^4	1.3
MHX	100	3.5×10^5	8.3	8.4×10^4	1.3
	10	9.9×10^4	25	1.6×10^4	3.2
MBA	100	3.6×10^5	7.9	2.8×10^5	5.8
1-PT	500	3.3×10^6	4.1	4.3×10^6	5.8

Table 2. $\langle N \rangle^{amp}$ for Ferrocene Species in ACN[a]

molecule (1 mM)	diffusion constant (m^2/s)	f_0^{meas} (Hz)	$\langle N \rangle^{freq}$	$\langle N_{ads} \rangle / \langle N_{sol} \rangle$	$\langle N \rangle^{amp}$	$\langle N_{ads} \rangle / \langle N_{sol} \rangle$
Fc	2.4×10^{-9}	1.31	2.21×10^6	2.76	1.90×10^6	2.24
Fc(MeOH)	1.94×10^{-9}	1.10	2.12×10^6	2.62	1.89×10^6	2.22
$Fc(MeOH)_2$	1.74×10^{-9}	0.95	2.21×10^6	2.76	1.92×10^6	2.27

[a] Experiments were performed in Type 1 devices with z = 65 nm.

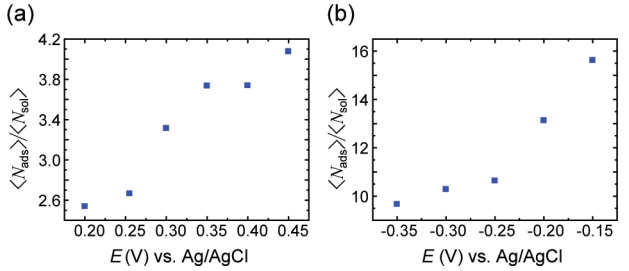

Figure 4. $\langle N \rangle^{amp}$ as a function of applied potential for aqueous solutions of (a) 0.5 mM $Fc(MeOH)_2$ ($E^{0\prime}$ = + 0.252 V) and (b) 0.5 mM $Ru(NH_3)_6^{3+}$ ($E^{0\prime}$ = −0.172 V). Experiments were performed with Type 2 devices.

adsorption is dependent on the potential applied, with a ∼ 50% increase in adsorption upon going from potentials that are below the half-wave potential to potentials that correspond to diffusion-limited currents. These results have an interesting implication for single-molecule redox cycling experiments. While adsorption does not affect the overall steady-state current, it does diminish the current-per-molecule, i_p.[12] The potential dependence of the adsorption suggests that, counterintuitively, the maximum sensitivity to single-molecule detection does not necessarily occur at high overpotentials.

CONCLUSIONS

In summary, we have introduced a simple method to measure dynamic adsorption at electrode systems that enclose small fluidic volumes based on amplitude measurements and/or cross-correlation analysis. Adsorption is revealed through a decrease in the amplitude of the fluctuations in the current. The method is equivalent to a frequency-based method introduced earlier, but crucially, the present analysis is more generally applicable and much simpler than the frequency-based method and easier to implement. In particular, a priori knowledge of the diffusion constants of the molecules and the exact geometry of the electrode setup is not required. Thus, while we have concentrated here on nanofluidic thin-layer cells, the method can be easily extended to other systems such as interdigitated electrodes embedded in nanochannels and scanning electrochemical microscopy (SECM). In the latter case, it is conceivable that this simple approach could be used to image spatially differing adsorption at patterned surfaces, especially in conjunction with the use of nanoelectrodes as tips.

Using the new method, we found that functionalizing the electrodes with self-assembled monolayers with polar end groups can reduce adsorption of $Fc(MeOH)_2$ onto Pt electrodes from aqueous solutions. The adsorption of molecules on metal electrode surfaces is a very complex process dependent on a variety of factors such as the electronic structure of the metal interface, the nature of the supporting electrolyte and of the adsorbate, and in many cases the potential of the electrode.[34,35] The proposed method offers a simple yet powerful tool to investigate how these parameters affect the presence and extent of adsorption. It can, therefore, offer insights into the rational design of surface modifications to minimize adsorption in nanofluidic channels.

ASSOCIATED CONTENT

Supporting Information. Text describing SAM formation, capacitances, and kinetics and the derivation of eq 2, and figures showing capacitive and redox cycling voltammograms related to characterization of SAMs, and a table listing double layer capacitances for the top electrode of various SAMs. This material is available free of charge via the Internet at http://pubs.acs.org.

AUTHOR INFORMATION

Corresponding Author
s.g.lemay@utwente.nl

ACKNOWLEDGMENT

We thank Dr. Anando Devadoss for helpful suggestions regarding SAM functionalization on metal electrodes. Funding by NWO and NanoNed are gratefully acknowledged.

REFERENCES

(1) Bohn, P. W. *Annu. Rev. Anal. Chem.* **2009**, *2*, 279–296.
(2) Kovarik, M. L.; Jacobson, S. C. *Anal. Chem.* **2009**, *81*, 7133–7140.

(3) Squires, T. M.; Messinger, R. J.; Manalis, S. R. *Nat. Biotechnol.* **2008**, *26*, 417–426.
(4) Zevenbergen, M. A. G.; Singh, P. S.; Goluch, E. D.; Wolfrum, B. L.; Lemay, S. G. *Nano Lett.* **2011**, *11*, 2881–2886.
(5) De Santo, I.; Causa, F.; Netti, P. A. *Anal. Chem.* **2010**, *82*, 997–1005.
(6) Durand, N. F.; Dellagiacoma, C.; Goetschmann, R.; Bertsch, A.; Märki, I.; Lasser, T.; Renaud, P. *Anal. Chem.* **2009**, *81*, 5407–5412.
(7) Durand, N. F. Y.; Bertsch, A.; Todorova, M.; Renaud, P. *Appl. Phys. Lett.* **2007**, *91*, No. 203106.
(8) Bard, A. J.; Faulkner, L. R. *Electrochemical Methods: Fundamentals and Applications*; Wiley: New York, 2001.
(9) Bond, A. M.; McLennan, E. A.; Stojanovic, R. S.; Thomas, F. G. *Anal. Chem.* **1987**, *59*, 2853–2860.
(10) Unwin, P. R.; Bard, A. J. *J. Phys. Chem.* **1992**, *96*, 5035–5045.
(11) Rodríguez-López, J.; Bard, A. J. *J. Am. Chem. Soc.* **2010**, *132*, 5121–5129.
(12) Zevenbergen, M. A. G.; Singh, P. S.; Goluch, E. D.; Wolfrum, B. L.; Lemay, S. G. *Anal. Chem.* **2009**, *81*, 8203–8212.
(13) Prime, K.; Whitesides, G. *Science* **1991**, *252*, 1164–1167.
(14) Ko, B. S.; Babcock, B.; Jennings, G. K.; Tilden, S. G.; Peterson, R. R.; Cliffel, D.; Greenbaum, E. *Langmuir* **2004**, *20*, 4033–4038.
(15) Fan, H.; López, G. P. *Langmuir* **1997**, *13*, 119–121.
(16) Sardar, R.; Beasley, C. A.; Murray, R. W. *Anal. Chem.* **2009**, *81*, 6960–6965.
(17) Lee, S.; Yoon, J. H.; Yoon, S. *J. Phys. Chem. C* **2011**, *115*, 12501–12507.
(18) Boschkova, K.; Stålgren, J. J. R. *Langmuir* **2002**, *18*, 6802–6806.
(19) Cutress, I. J.; Dickinson, E. J.; Compton, R. G. *J. Electroanal. Chem.* **2011**, *655*, 1–8.
(20) Singh, P. S., et al. Unpublished results, 2011
(21) Love, J. C.; Estroff, L. A.; Kriebel, J. K.; Nuzzo, R. G.; Whitesides, G. M. *Chem. Rev.* **2005**, *105*, 1103–1170.
(22) Stern, D. A.; Wellner, E.; Salaita, G. N.; Laguren-Davidson, L.; Lu, F.; Batina, N.; Frank, D. G.; Zapien, D. C.; Walton, N.; Hubbard, A. T. *J. Am. Chem. Soc.* **1988**, *110*, 4885–4893.
(23) Lin, T. H.; Huang, T. P.; Liu, Y. L.; Yeh, C. C.; Lai, Y. H.; Hung, W. H. *J. Phys. Chem. B* **2005**, *109*, 14079–14084.
(24) Lang, P.; Mekhalif, Z.; Rat, B.; Gamier, F. *J. Electroanal. Chem.* **1998**, *441*, 83–93.
(25) Petrovykh, D. Y.; Kimura-Suda, H.; Opdahl, A.; Richter, L. J.; Tarlov, M. J.; Whitman, L. J. *Langmuir* **2006**, *22*, 2578–2587.
(26) Laiho, T.; Leiro, J. A.; Lukkari, J. *Appl. Surf. Sci.* **2003**, *212−213*, 525–529.
(27) Li, Z.; Chang, S.-C.; Williams, R. S. *Langmuir* **2003**, *19*, 6744–6749.
(28) Zevenbergen, M. A. G.; Wolfrum, B. L.; Goluch, E. D.; Singh, P. S.; Lemay, S. G. *J. Am. Chem. Soc.* **2009**, *131*, 11471–11477.
(29) Brito, R.; Tremont, R.; Feliciano, O.; Cabrera, C. R. *J. Electroanal. Chem.* **2003**, *540*, 53–59.
(30) Malem, F.; Mandler, D. *Anal. Chem.* **1993**, *65*, 37–41.
(31) Spégel, C.; Heiskanen, A.; Acklid, J.; Wolff, A.; Taboryski, R.; Emnéus, J.; Ruzgas, T. *Electroanalysis* **2007**, *19*, 263–271.
(32) Finklea, H. O.; Avery, S.; Lynch, M.; Furtsch, T. *Langmuir* **1987**, *3*, 409–413.
(33) Porter, M. D.; Bright, T. B.; Allara, D. L.; Chidsey, C. E. D. *J. Am. Chem. Soc.* **1987**, *109*, 3559–3568.
(34) Magnussen, O. M. *Chem. Rev.* **2002**, *102*, 679–726.
(35) Tripkovic, D. V.; Strmcnik, D.; van der Vliet, D.; Stamenkovic, V.; Markovic, N. M. *Faraday Discuss.* **2009**, *140*, 25–40.